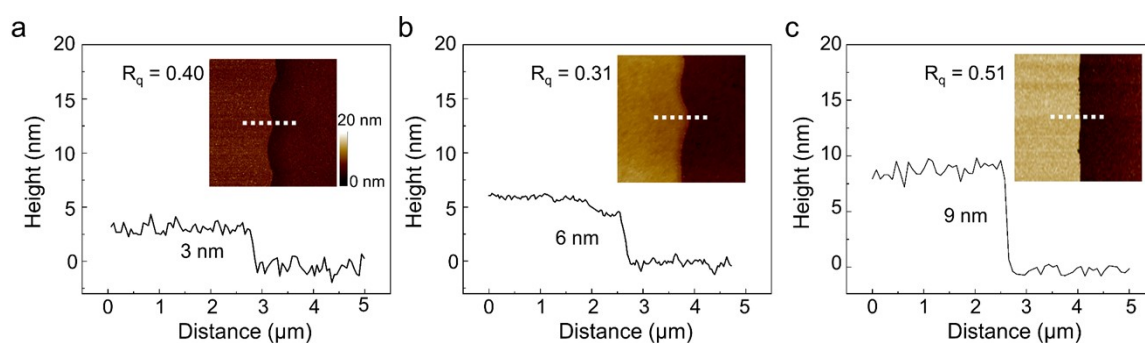


## Electronic Supplementary Information (ESI)

### Light-induced tunable threshold voltage and synaptic behavior of solution-processed indium oxide thin film transistor for logic computing and image denoising

*Pengsheng Li, Zixu Sa, Zeqi Zang, Guangcan Wang, Mingxu Wang, Lei Liao, Feng Chen, and Zai-xing Yang*



**Fig. S1.** The thicknesses of  $\text{In}_2\text{O}_3$  thin films. (a) 1 layer, (b) 2 layers and (c) 3 layers. Insets are AFM images

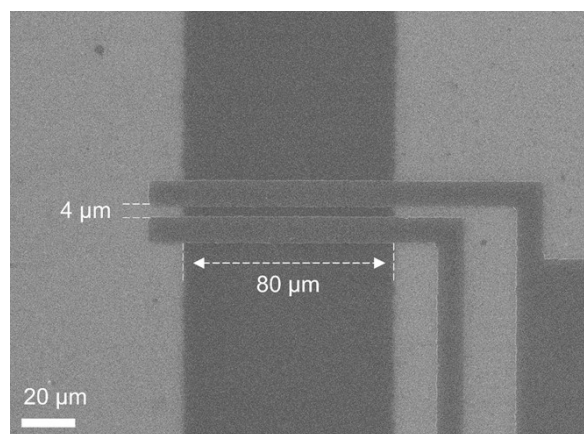


**Fig. S2.** The SEM image of  $\text{In}_2\text{O}_3$  TFT.

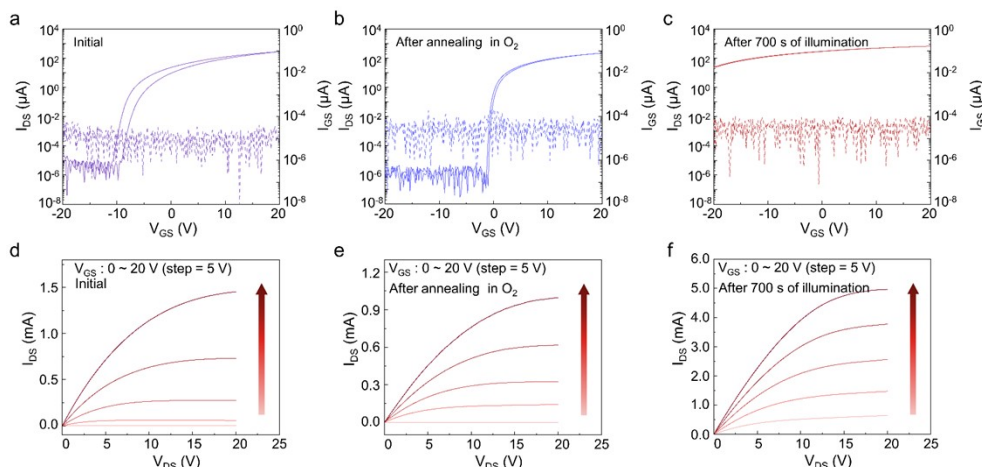


**Fig. S3.** Output curves of  $\text{In}_2\text{O}_3$  TFT in (a) initial state, (b) after annealing in oxygen. Fig. S3 shows the transfer and output curves of the  $\text{In}_2\text{O}_3$  TFT in its initial state, after annealing in oxygen, and after 700 s of illumination. Obviously, from Fig. S3a-c, the leakage currents ( $I_{GS}$ ) of the  $\text{In}_2\text{O}_3$  TFT are significantly smaller than the source-drain currents ( $I_{DS}$ ). At the same time,  $\text{In}_2\text{O}_3$  TFTs maintain good ohmic contact in all conditions, as shown in Fig. S3d-f.

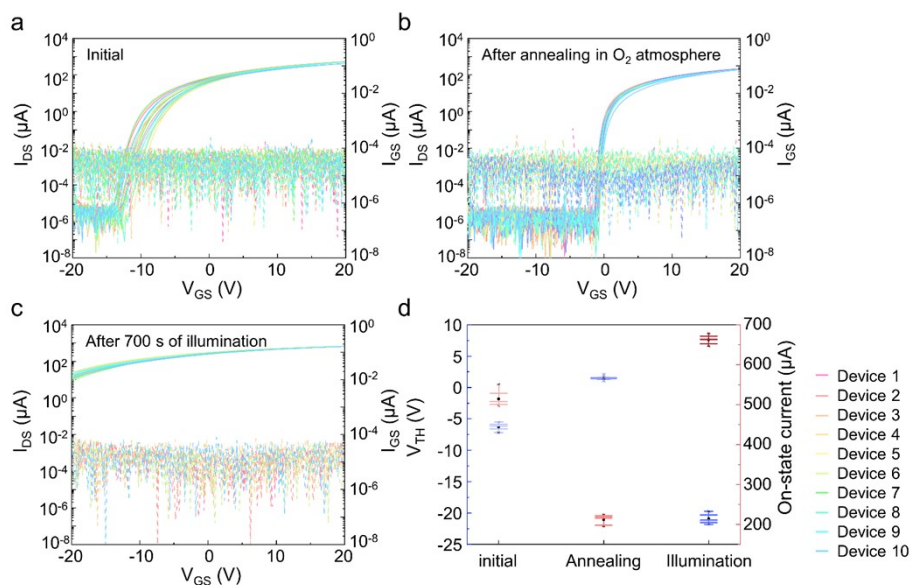


**Fig. S4.** Statistical data on the variation in  $V_{TH}$  of  $\text{In}_2\text{O}_3$  TFT in the (a) initial state and (b) after annealing in oxygen and (c) after 700 s of illumination. (d)  $V_{TH}$  and on-state current statistics of  $\text{In}_2\text{O}_3$  TFT in initial state, after annealing in  $\text{O}_2$  and after 700 s of illumination.

As shown in the transfer curves of Fig. S4a, the transfer curves of as-fabricated  $\text{In}_2\text{O}_3$  TFTs demonstrate the depletion operation mode with average  $V_{\text{TH}}$  of approximately -6.3 V and average on-state current of 514  $\mu\text{A}$ . After annealing in  $\text{O}_2$  atmosphere, the transfer curves of Fig. S4b show that the  $V_{\text{TH}}$  of  $\text{In}_2\text{O}_3$  TFTs shift to 1.5 V, along with the transition from depletion operation mode to enhancement operation mode. At the same time, the on-state currents decrease to 213  $\mu\text{A}$ . With the illumination times increase to 700 s, the 10 TFTs show  $V_{\text{TH}}$  of - 21.7 V and on-state currents of 662  $\mu\text{A}$ , as shown in Fig. S4c. The leakage currents of all TFTs are  $\sim 10^{-11}$   $\mu\text{A}$ . Fig. S4d shows the  $V_{\text{TH}}$  statistics and on-state currents of 10  $\text{In}_2\text{O}_3$  TFTs under three conditions. Obviously, all the solution-processed amorphous  $\text{In}_2\text{O}_3$  TFTs show neglected deviations in  $V_{\text{TH}}$  and on-state currents under three conditions, implying the excellent reproducibility and reliability.

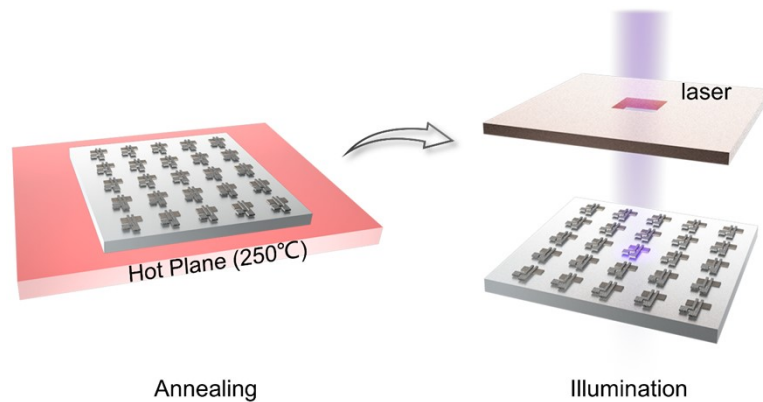


**Fig. S5.** Schematic diagram of annealing-illumination combined method for the precise regulation of  $V_{\text{TH}}$  of solution-processed  $\text{In}_2\text{O}_3$  TFTs.

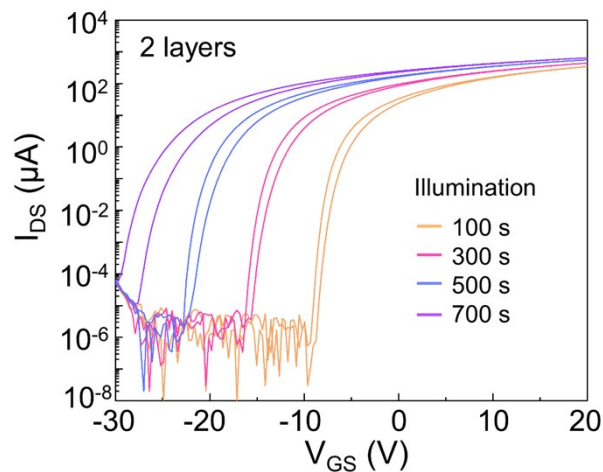


**Fig. S6.** Transfer curves of annealed In<sub>2</sub>O<sub>3</sub> 2 layers TFT under the illumination times of 100 s, 300 s, 500 s and 700 s with power intensity of 0.29 mW/mm<sup>2</sup>.

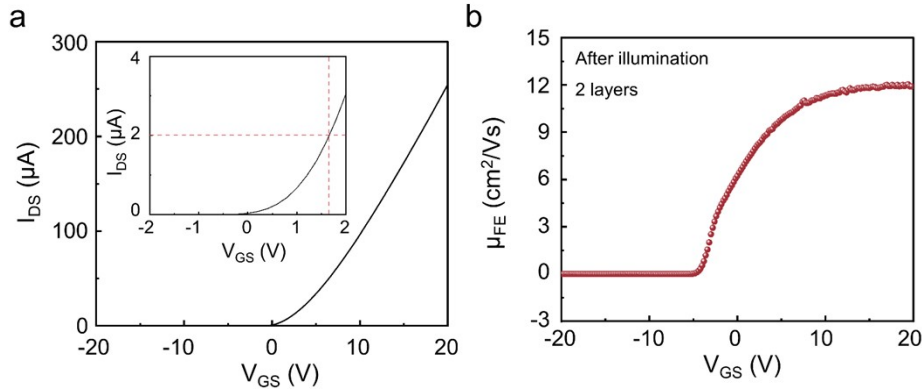


**Fig. S7.** Extraction methods of threshold voltage and field-effect peak mobility.

In this work, the threshold voltage ( $V_{TH}$ ) is determined as the gate voltage ( $V_{GS}$ ) at which the  $I_{DS}$  reaches to  $W/L \times 100$  nA.<sup>1-3</sup> At the same time, the field-effect peak mobility ( $\mu_{FE}$ ) is obtained from the formula of  $\mu_{FE} = Lg_m / WC_{OX}V_{DS}$ , where  $L$  is channel length,  $g_m$  is maximum transconductance,  $W$  is the channel width,  $C_{OX}$  is the gate capacitance.<sup>4</sup>

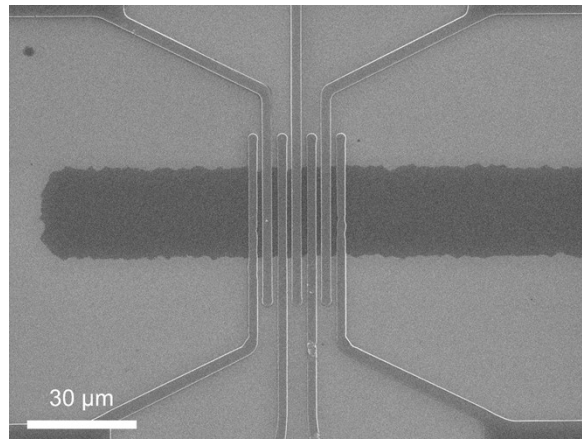


**Fig. S8.** SEM image of In<sub>2</sub>O<sub>3</sub> top-gate TFT.

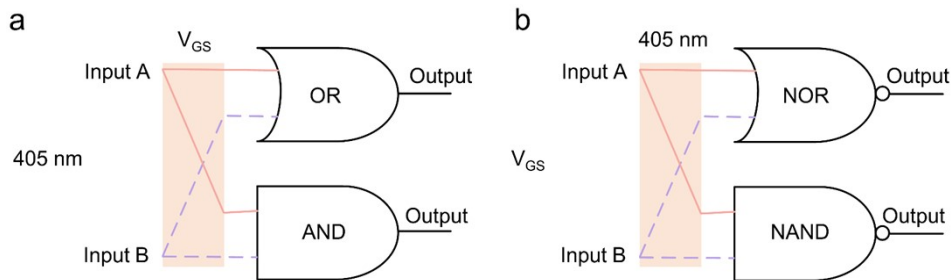


**Fig. S9.** Schematic operation diagram for the logic functions of (a) “OR”, “AND” (b) “NOR”, “NAND” in the optoelectronic synapse.

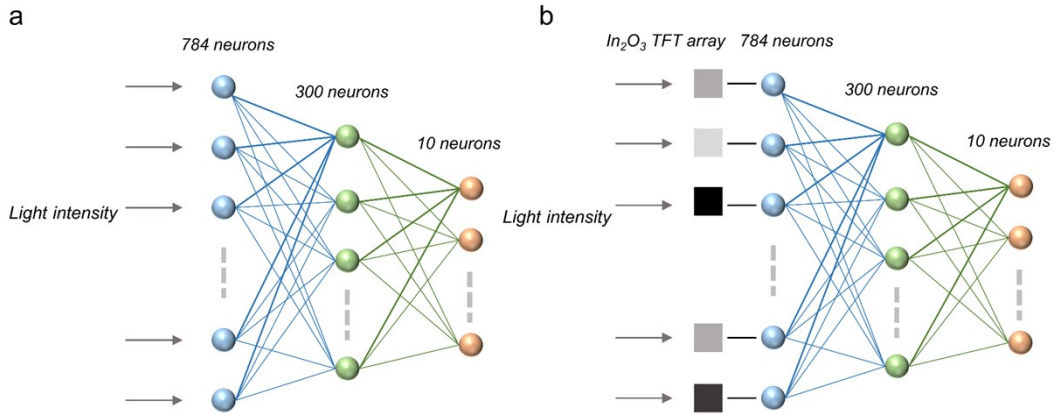


**Fig. S10.** (a) The structure of the three-layered artificial neural network without  $\text{In}_2\text{O}_3$  TFTs array. (b) The structure of the three-layered artificial neural network with  $\text{In}_2\text{O}_3$  TFTs array.

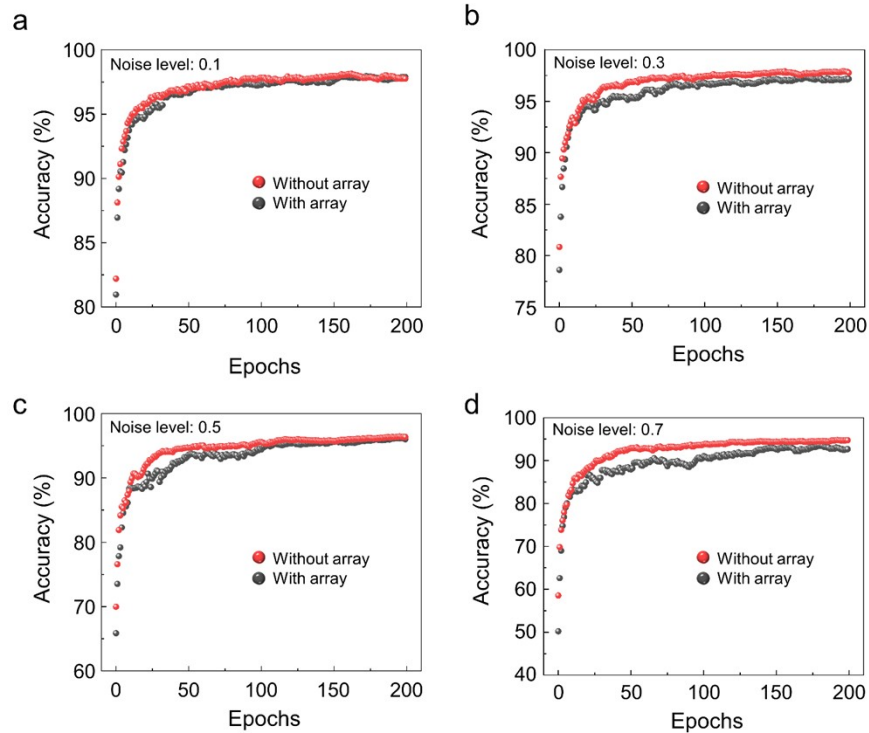


**Fig. S11.** The recognition rate with or without  $\text{In}_2\text{O}_3$  TFTs array under the noise levels of 0.1, 0.3, 0.5, and 0.7.

Taking into account the increase in efficiency of the recognition task using  $\text{In}_2\text{O}_3$  TFTs array, the number of epochs required to achieve different recognition accuracies, with and without the  $\text{In}_2\text{O}_3$  TFTs array, is extracted from the simulation. Due to the similar structure of neural networks with  $\text{In}_2\text{O}_3$  TFTs array and without  $\text{In}_2\text{O}_3$  TFTs array, the power consumption and speed of a single epoch are roughly equal. Therefore, for the same

accuracy, the entire processing speed is inversely proportional to the epoch, and the entire energy consumption is proportional to the epoch. The improvement rate is defined as:<sup>5</sup>

Rate of improvement (%) = (Epochs (without array) – Epochs (with array)) / Epochs (without array) × 100%.

## Reference

- 1 Y. Zheng, S. Ghosh, S. Das, *Adv. Mater.*, 2024, **36**, e2307380.
- 2 D. Kang, J. T. Jang, S. Park, M. H. R. Ansari, J.-H. Bae, S.-J. Choi, D. M. Kim, C. Kim, S. Cho, D. H. Kim, *IEEE Access*, 2021, **9**, 59345-59352.
- 3 M. Bucher, N. Makris, L. Chevas, *IEEE Trans. Electron Devices*, 2020, **67**, 4559-4562.
- 4 W. Wang, L. Li, C. Lu, Y. Liu, H. Lv, G. Xu, Z. Ji, M. Liu, *Appl. Phys. Lett.*, 2015, **107**.
- 5 F. Zhou, Z. Zhou, J. Chen, T. H. Choy, J. Wang, N. Zhang, Z. Lin, S. Yu, J. Kang, H. S. P. Wong, Y. Chai, *Nat. Nanotechnol.*, 2019, **14**, 776-782.